

Systematic Search and A New Family of Skyrmion Materials

Wei Li¹ and Jiadong Zang^{2,*}

¹*State Key Laboratory of Functional Materials for Informatics and Shanghai Center for Superconductivity,
Shanghai Institute of Microsystem and Information Technology,
Chinese Academy of Sciences, Shanghai 200050, China*

²*Institute for Quantum Matter, Department of Physics and Astronomy,
Johns Hopkins University, Baltimore, Maryland 21218, USA*

(Dated: June 15, 2021)

Magnetic skyrmions have recently attracted great attentions. However they are harbored in very limited numbers of magnets up to now. The search of new helimagnetic materials is thus an urgent topic in the field of skyrmion physics. In this letter, we provide a guideline on this issue, and discuss the possibility of realizing skyrmions in a new family of molybdenum nitrides $A_2\text{Mo}_3\text{N}$ ($A=\text{Fe}, \text{Co},$ and Rh). By means of the first-principles calculations, the electronic and magnetic structures are calculated and the existence of strong Dzyaloshinskii-Moriya interaction is demonstrated.

PACS numbers: 75.10.Hk, 75.50.-y, 71.20.-b

The magnetic skyrmion is a swirling-like spin texture with nontrivial topology, where magnetic moments point in all directions in the space, in contrast to any other trivial textures such as ferromagnetism. Soon after its first encounter with magnetism [1], the skyrmion was observed in MnSi by neutron scattering [2], and later confirmed in $\text{Fe}_{1-x}\text{Co}_x\text{Si}$ by Lorentz transmission electron microscopy [3]. It has attracted great attentions due to its promise of future applications in memory devices [4]. Recent developments have witnessed skyrmions in several other bulk materials, such as FeGe [5], hosting skyrmions quite close to room temperatures, and Cu_2OSeO_3 [6], where skyrmions are insulating and exhibiting multiferroic properties.

However all these materials belong to the same lattice class called B20 compounds in the Strukturbericht Symbol. Although this class belongs to the cubic crystal system, complicated distributions of atoms in each unit cell dramatically bring down the symmetry. Thus the point group of B20 compounds is the tetartoidal T23 group, the one with lowest symmetry in the cubic system, where both inversion and mirror symmetries are missing. It has been well understood that the inversion symmetry breaking generates the Dzyaloshinskii-Moriya (DM) interaction [7, 8], which competes with the Heisenberg exchange, and induces skyrmions or conical state at finite magnetic fields. This competition is also the origin of the spin helices under low magnetic fields [9]. That is why B20 compounds are termed as helimagnets. The DM interaction is noticeably large in B20 compounds, so that the dipolar interaction is negligible. This provides skyrmions therein with the same chirality and controllable properties. Facing the limited choices of B20 compounds, an urgent problem thus arises that how to find other helimagnet materials harboring skyrmions, spin helices, or conical states driven by the DM interaction.

In B20 helimagnets, the essential Hamiltonian in the

continuum limit is given by

$$H = J(\nabla\mathbf{S})^2 + D\mathbf{S} \cdot (\nabla \times \mathbf{S}) - \mathbf{h} \cdot \mathbf{S} \quad (1)$$

It has been extensively tested this Hamiltonian well characterizes the phase diagrams of the B20 compounds. The last term in Eq. (1) is the Zeeman coupling. At a finite window of the magnetic field and temperature, the skyrmion would appear, while the helix is energetically favored at low magnetic fields. The presence of the helix can be readily understood by visiting the leading two terms, the Heisenberg exchange and the DM interaction respectively, in Eq. (1). One can perform the Fourier transformation of the Hamiltonian, and get a quadratic function in momentum \mathbf{k} from the Heisenberg exchange, while receiving a linear function in momentum from the DM interaction. The Hamiltonian is thus minimized at a finite momentum \mathbf{k}_0 , which is the wavevector of spin helix. It shows a linear term in momentum is essential.

In details, the Fourier component of the Heisenberg exchange is given by $H_{\text{Hei}}(\mathbf{k}) = J\mathbf{k}^2|\mathbf{S}_{\mathbf{k}}|^2$, where $\mathbf{S}_{\mathbf{k}}$ is the Fourier component of the spin $\mathbf{S}_{\mathbf{k}} = \frac{1}{V} \int d\mathbf{r} \mathbf{S}(\mathbf{r}) \exp(i\mathbf{k} \cdot \mathbf{r})$. Under rotations, \mathbf{S} transforms in the same way as \mathbf{k} . As a result, $H_{\text{Hei}}(\mathbf{k})$ is rotationally invariant. Furthermore, inversion and mirror symmetries are also respected. Therefore this is a generic quadratic term for all ferromagnets.

On the other hand, the DM interaction provides a linear term in momentum; $H_{\text{DM}}(\mathbf{k}) = iD\mathbf{S}_{\mathbf{k}} \cdot (\mathbf{k} \times \mathbf{S}_{-\mathbf{k}})$. Although the rotational symmetry is still preserved, inversion symmetry is apparently broken, which is the well know precondition for the DM interactions. However a long overlooked fact is the mirror symmetry is also broken by this DM interaction. This comes from the fact that $\mathbf{S}_{\mathbf{k}} \cdot (\mathbf{k} \times \mathbf{S}_{-\mathbf{k}})$ is a pseudoscalar. Under any improper rotation such as mirror reflection in the lattice, this term flips sign, and should be ruled out in the energy. That is why magic is witnessed in B20 compounds. The point group T23 only has pure rotations, thus al-

lows the DM interaction in this form. In case a mirror plane exists, the DM interaction arise from broken inversion symmetry must be staggered, failing to end up with a continuum limit in this form. Now a question arises whether this form is the only allowed term linear in \mathbf{k} for any materials.

To answer this question, we can rewrite any \mathbf{k} -linear terms as a tensor product $H_{\text{DM}}(\mathbf{k}) = id_{ijm}k^iS_{-\mathbf{k}}^jS_{\mathbf{k}}^m$, where d_{ijm} is a third order tensor that can be constructed from symmetry analysis. Any symmetry operation R can be represented as a 3×3 matrix in natural basis (x, y, z). Under such operation, vector \mathbf{k} transforms as $k_i \rightarrow k_j R_{ji}$, while the pseudovectors $\mathbf{S}_{\pm\mathbf{k}}$ transform as $S_i \rightarrow |R|S_j R_{ji}$, where $|R|$ is the determinant of R matrix. If R is an improper rotation, $|R| = -1$. Once R is a symmetry operation, energy should be invariant under such rotation, therefore the tensor d_{ijm} must satisfy the Neumann's principle:

$$d_{ijm} = R_{ip}R_{jq}R_{mr}d_{pqr} \quad (2)$$

In practice, one does not need to go through all symmetry operations in order to determine the d tensor. Most operations can be written as products of some independent matrices, called generating matrices [10], within the same point group. For T23 point group, the generating matrices are C_2 and C_3 rotations. The Neumann's principle thus leads to the constrain that $d_{xyz} = d_{yzx} = d_{zxy}$, and $d_{xzy} = d_{yxz} = d_{zyx}$. One can symmetrize these parameters by $d_{xyz} = S + D$ and $d_{xzy} = S - D$. However because the whole Hamiltonian can be reorganized as $\sum_{\mathbf{k}} H_{\text{DM}}(\mathbf{k}) = \sum_{\mathbf{k}} i(d_{ijm} - d_{imj})k^iS_{-\mathbf{k}}^jS_{\mathbf{k}}^m$, the symmetric component S does not contribute. The resulting Hamiltonian is thus $\sum_{\mathbf{k}} iD\varepsilon_{ijm}k^iS_{-\mathbf{k}}^jS_{\mathbf{k}}^m$, which reproduces the DM interaction in Eq. (1).

The same method applies to any other lattices. Contribution to the Hamiltonian from any tensor with redundant indices vanishes when completing the summation over momenta. The relevant terms are six components with indices permutations of (x, y, z). For future convenience, these six components are symmetrized as $d_{xyz} = \alpha_S + \alpha_A$, $d_{yxz} = \alpha_S - \alpha_A$, $d_{yzx} = \beta_S + \beta_A$, $d_{xzy} = \beta_S - \beta_A$, $d_{zxy} = \gamma_S + \gamma_A$, $d_{zyx} = \gamma_S - \gamma_A$. As a result, the total Hamiltonian is given by

$$\begin{aligned} H = \int d^3\mathbf{r} \quad & [J(\nabla\mathbf{S})^2 - \mathbf{h} \cdot \mathbf{S} \\ & + \frac{1}{2}(\alpha_S + \alpha_A - \beta_S + \beta_A)\mathbf{S} \cdot (\partial_{\hat{x}} \times \mathbf{S}) \\ & + \frac{1}{2}(-\alpha_S + \alpha_A + \beta_S + \beta_A)\mathbf{S} \cdot (\partial_{\hat{y}} \times \mathbf{S}) \\ & + \gamma_A\mathbf{S} \cdot (\partial_{\hat{z}} \times \mathbf{S})] \end{aligned} \quad (3)$$

where $\partial_{\hat{r}}$ is the directional derivative along \mathbf{r} direction. Under low magnetic field \mathbf{h} , spin helix is thus formed along certain directions given the competition between anisotropic DM interaction and the Heisenberg exchange.

TABLE I: Constrains of nonzero d_{ijk} parameters for all possible point groups

Class	Constrains	Point Groups
I	No Constrain	C_1, C_2, D_2
II	$\alpha_S = \beta_S = \gamma_S = 0$	$C_4, D_4, C_3, D_3, C_6, D_6$
III	$\alpha_A = \beta_A = \gamma_A = 0$	S_4, D_{2d}
IV	$\alpha_S = \beta_S = \gamma_S, \alpha_A = \beta_A = \gamma_A$	T
V	$\alpha_S = \beta_S = \gamma_S = 0, \alpha_A = \beta_A = \gamma_A$	O

A complete list of point groups contributing to nonzero DM interactions is summarized in Table I, where the B20 compounds are located in class-IV. We know that the point group can be decomposed into two categories, the ones with and without improper rotations. Most groups in Table I belong to the category without any improper rotations. Mirror, in addition to inversion, is broken in these lattices. The only exception is class-III; S_4 and D_{2d} groups, where $\mathbf{S} \cdot (\partial_{\hat{z}} \times \mathbf{S})$ is prohibited. Helices or skyrmions can only form in the plane perpendicular within the horizontal mirror. In contrast, class-II allows the presence of the DM interaction in the z -direction. The DM interaction of this class can be rewritten as $\frac{1}{2}(\alpha_A + \beta_A + \gamma_A)\mathbf{S} \cdot (\nabla \times \mathbf{S}) + \frac{1}{2}\gamma_A\mathbf{S} \cdot (\partial_{\hat{z}} \times \mathbf{S})$. It shows explicitly that the z -direction is distinct from the xy plane. Although helices or conics can propagate along z -direction, the skyrmion crystal would favor to accommodate in the xy plane instead. However one should be aware that the spin anisotropies are quite large in these lattices with reduced symmetry, which are enemies of the skyrmion. One can also construct spin anisotropies by the symmetry tensors up to arbitrary order. These details are out of the scope of this work. In the future, case by case studies can be conducted for specific materials.

The most important message delivered from Table I is class-V, which is described by *exactly the same* Hamiltonian as the B20 compounds in class-IV. The spin anisotropies are also the same in these two classes. Therefore we expect the spin physics observed in B20 compounds are also persistent in the point group O . There exists 8 space groups in O group. We found that the most promising material in analogy to B20 compounds is the $A_2\text{Mo}_3\text{N}$ family with $A=\text{Fe, Co, Rh}$, or their alloys. The pure $A_2\text{Mo}_3\text{N}$ [13–15], shown in Fig. 1(a), has the filled β -manganese structure, where A atoms lie on the 8c positions of a cubic unit cell with space group symmetry $P4_132$ forming a single (10, 3)-a network [16]. The space within this network is filled by corner-shared Mo_6N octahedra. This structure is entirely analogous to that of β -manganese, differing only by the addition of the interstitial non-metal atoms. We expect large strength of spin-orbital coupling in this family, and thus skyrmions can be hosted.

To quantitatively confirm the aforementioned conjecture of promising material, we carried out the first-principle calculations of pure $A_2\text{Mo}_3\text{N}$ using the pro-

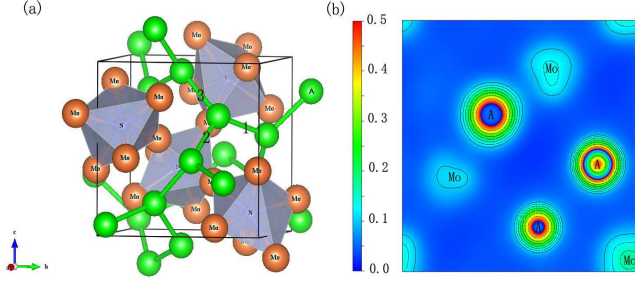


FIG. 1: (Color online) (a) The schematic crystal structure of the filled β -manganese structural A_2Mo_3N ($A=Co, Fe$, and Rh). Space within the $(10, 3)$ -a network of A atoms (green) is filled by vertex-sharing Mo_6N . (b) The charge density distribution in the (001) plane crossing the A - Mo - A atoms in the NM state calculations.

jected augmented wave method as implemented in the VASP code [11], where the exchange-correlation potential was calculated using the generalized gradient approximation (GGA) as proposed by Pedrew, Burke, and Ernzerhof (PBE) [12]. All atomic positions and lattice constants of A_2Mo_3N were allowed to relax simultaneously to minimize the energy. A 500 eV cutoff in the plane wave expansion ensures the convergence of calculations up to 10^{-5} eV, and all atomic positions and the lattice constants were optimized until the largest force on any atom was 0.005 eV/Å. Furthermore, we used a $8 \times 8 \times 8$ Monkhorst-Pack k-grid Brillouin zone sampling throughout all of calculations. In addition, the spin-orbit coupling was also included with the second variational method. The lattice constants and the internal coordinates of the atomic positions for the systems of A_2Mo_3N are all optimized and listed in Table II, which shows that the optimized lattice parameters for both Fe_2Mo_3N and Co_2Mo_3N are quite consistent with that from experiments [13–15]. Although lattice parameters for Rh_2Mo_3N are lacking experimentally, our optimized values are larger than those of Fe_2Mo_3N and Co_2Mo_3N , which are reasonable as the atomic radii of Rh is apparently larger than that for Fe and Co .

The electronic properties of A_2Mo_3N in the quenched paramagnetic state in A 3(4) d and Mo 4 d orbitals are studied. Such studies provide references for forthcoming magnetism studies. By analyzing the density of states

TABLE II: The optimized lattice constants as well as the internal coordinates for the filled β -manganese structured A_2Mo_3N ($A=Co, Fe$, and Rh).

A_2Mo_3N	$A=Fe$	$A=Co$	$A=Rh$
a (Å)	6.6458	6.6367	6.8224
A ($\hat{x} = \hat{y} = \hat{z}$)	0.0723	0.0677	0.0598
Mo (\hat{y})	0.2019	0.2002	0.2021
Mo (\hat{z})	0.4519	0.4502	0.4521

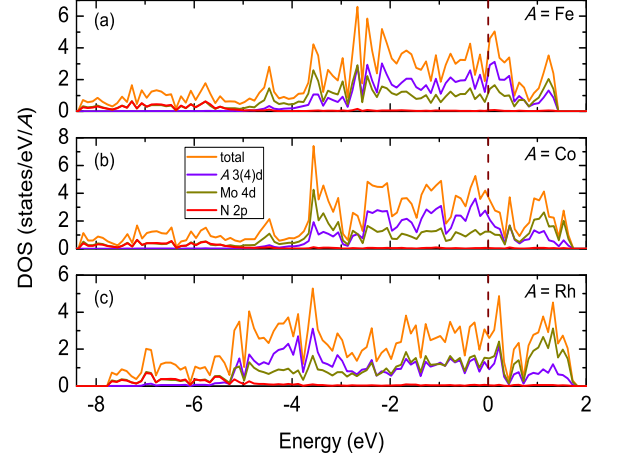


FIG. 2: (color online) Total DOS and PDOS on A 3(4) d , Mo 4 d , and N 2 p orbitals of the NM state for A_2Mo_3N with (a) $A=Fe$, (b) $A=Co$, and (c) $A=Rh$. The Fermi energies are set to zero.

(DOS) at the Fermi level we can infer whether the magnetic state is favored. Fig. 2 shows the total DOS of A_2Mo_3N , and its projected DOS (PDOS) onto A 3(4) d , Mo 4 d , and N 2 p orbitals respectively. Furthermore, it also shows that the mixing between A 3(4) d and Mo 4 d occurs mainly around the Fermi energy ranging from -4 eV to 2 eV indicating the sizable 3(4) d -4 d hybridization between A 3(4) d and Mo 4 d orbitals. Particularly, comparable contributions to the conducting carriers are witnessed from the Rh 4 d and Mo 4 d orbitals in Rh_2Mo_3N , shown in Fig. 2(c). This is attributed to the much more extended 4 d orbitals of Rh compared to the 3 d orbitals of Fe and Co , which leads to a stronger hybridization, expanded bandwidth, and highly overlapping between Rh 4 d and Mo 4 d orbital states. Additionally, it is important to point out that the DOS coming from A 3(4) d orbitals is nonvanishing at the Fermi level. The values of DOS at the Fermi level are $[N_{Fe}^{Fe}(E_f) = 2.4$ and $N_{Mo}^{Fe}(E_f) = 0.73]$, $[N_{Co}^{Co}(E_f) = 2.3$ and $N_{Mo}^{Co}(E_f) = 0.8]$, and $[N_{Rh}^{Rh}(E_f) = 1.5$ and $N_{Mo}^{Rh}(E_f) = 0.67]$ states per eV per $A(Mo)$ atom for Fe_2Mo_3N , Co_2Mo_3N , and Rh_2Mo_3N , respectively. According to the Stoner criterion [17, 18], magnetism may occur only when the DOS satisfies $N(E_f)I > 1$, where I is the Stoner parameter, which takes values of 0.7 eV-0.9 eV for ions near the middle of the transition metal series (note that the effective I can be reduced by hybridization). It shows clearly that although the NM state is favorable on the Mo atoms, it is unstable against the magnetic states on the A atoms. A atoms are responsible for magnetisms in this family.

To explore the magnetic behaviors of A atoms in A_2Mo_3N , we consider a local exchange model based on

the nearest neighbor Heisenberg and DM interactions:

$$H = \sum_{\langle i,j \rangle} J_{ij} \mathbf{S}_i \cdot \mathbf{S}_j + \sum_{\langle i,j \rangle} \mathbf{D}_{ij} \cdot (\mathbf{S}_i \times \mathbf{S}_j), \quad (4)$$

where \mathbf{S}_i is the operator of A spin at site i , $\langle i, j \rangle$ denotes the summation over the nearest neighboring sites between A atoms. Parameters J_{ij} and \mathbf{D}_{ij} are the nearest neighbor Heisenberg and DM interactions, respectively, which can be evaluated by using the four-state energy-mapping analysis [19]. The results are listed in Table III. Here lists only the coupling constants on the three bonds shown in Fig. 1(a). Interactions on other bonds are the same except for a rotation. The vector \mathbf{D}_{ij} of the DM interaction on each bond are almost perpendicular to the bond as expected. That is because the lack of inversion symmetry generates a local electric field \mathbf{e} on each bond. An electron hopping between two ends of this bond mediates the exchange interaction of the neighboring spin, and feels an effective magnetic field $\mathbf{b} = \mathbf{v} \times \mathbf{e}$, where velocity \mathbf{v} is along the bond. Spin of this electron thus proceed about \mathbf{b} , resulting in a DM interaction of neighboring spins with the DM vector parallel \mathbf{b} . Therefore \mathbf{D}_{ij} should be perpendicular to the bond. The small deviation from perpendicular is associated with the non-uniformity of \mathbf{e} . The consistency between this physical picture and the calculation results justifies our evaluation of the DM interactions. From these data we notice that the Heisenberg interactions J_{ij} are almost the same on the three bonds in each compound. They reach the maximal value in $\text{Rh}_2\text{Mo}_3\text{N}$, which attributes to the nature of strong hybridization between Rh $4d$ and Mo $4d$ orbitals [see the charge density distribution shown in Fig. 1(b)]. The ratio between the DM interaction and Heisenberg exchange has the largest value $\gamma = |\frac{\mathbf{D}_{ij}}{J_{ij}}| \approx 0.084$ in $\text{Co}_2\text{Mo}_3\text{N}$, while that of $\text{Fe}_2\text{Mo}_3\text{N}$ and $\text{Rh}_2\text{Mo}_3\text{N}$ are 0.069 and 0.073, respectively. These values are much larger than conventional ratios of $\gamma < 0.05$ [8]. Such strong DM interaction between A - A atoms in $A_2\text{Mo}_3\text{N}$ mainly comes from strong spin-orbital coupling in Mo $4d$ orbitals, which mediate the spin-spin interaction between A atoms as indicated from the charge density distribution shown in Fig. 1(b). Thus, we conclude that the $\text{Co}_2\text{Mo}_3\text{N}$ with strong DM interaction is a promising candidate for realizing the exotic skyrmion in pure $A_2\text{Mo}_3\text{N}$ series.

As the skyrmion radius is controlled by the ratio between the DM interaction and Heisenberg exchange, it is of great interesting, from both physics and applications' perspectives, to find materials with large $\gamma = |\frac{\mathbf{D}_{ij}}{J_{ij}}|$. To this end, material optimizing is required. Here, we suggest that the substituted compound $\text{Co}_{2-x-y}\text{Rh}_x\text{Fe}_y\text{Mo}_3\text{N}$ has a larger γ value than pure $\text{Co}_2\text{Mo}_3\text{N}$ by fine tuning the stoichiometry. According to the aforementioned calculations and discussions, the strength of DM can be raised through an enhancement of the hybridization between A $3(4)d$ and Mo $4d$ orbitals.

TABLE III: The values of magnetic exchange coupling and DM interactions on the three bonds shown in Fig. 1(a) in the filled β -manganese structured $A_2\text{Mo}_3\text{N}$ ($A=\text{Co}$, Fe , and Rh). The unit is meV/S^2 , where S is the spin of the A atom.

	$A=\text{Fe}$	$A=\text{Co}$	$A=\text{Rh}$
J_1	-27.17	-41.46	-62.71
J_2	-27.23	-41.46	-62.85
J_3	-27.25	-41.46	-62.84
\mathbf{D}_1	(0.36,-0.37, 1.80)	(1.19,-1.16, 3.06)	(2.39,-2.50, 1.71)
\mathbf{D}_2	(-0.53, 0.61,-0.07)	(-1.05, 1.12, 2.69)	(-1.51, 1.26, 4.35)
\mathbf{D}_3	(0.61, 0.48, 0.08)	(1.11, 1.05,-2.69)	(2.02, 1.41,-4.31)

Therefore partially substituting Co by Rh will help as the $4d$ orbital of Rh is more extended than the $3d$ orbital of Co, which makes the overlapping to Mo $4d$ orbital more sufficient. However, such substitution simultaneously introduces large atomic orbital potential difference between large radii Rh and small radii Co atoms, which generates large scattering on itinerant electrons and weakens the exchange interactions. To overcome those potential barriers, an isovalent dopant Fe needs to be introduced. Based on this analysis we further calculate the magnetic exchange interactions for $\text{CoRh}_{0.75}\text{Fe}_{0.25}\text{Mo}_3\text{N}$ and obtain the ratio $\gamma = |\frac{\mathbf{D}_{ij}}{J_{ij}}|$ up to 0.11. Therefore, we suggest the substituted compound $\text{Co}_{2-x-y}\text{Rh}_x\text{Fe}_y\text{Mo}_3\text{N}$ is the most promising material realizing the exotic skyrmion state. An experimental hint has already been observed in [15], where zero remanence and a kink of magnetic susceptibility both indicate the presence of spin helices, the forerunner of skyrmions, at small magnetic fields and low temperatures. A complete exploration of the phase diagram and stoichiometry is required. On the other hand, the Curie temperature can be elevated by introducing other dopants such as Pt[14].

In conclusion, we have constructed a framework of searching new helimagnet materials harboring exotic spin textures of skyrmions. The effective Hamiltonian is derived based on symmetry analysis. A new family $A_2\text{Mo}_3\text{N}$ ($A=\text{Fe}$, Co , and Rh) has been proposed, and the first-principle calculations are performed. We hope that this family is just a corner of a huge iceberg.

We thank H. F. Du, C. L. Chien, M. H. Jiang, X. M. Xie, Z. Liu, and Y. Li for helpful discussions. WL was supported by the Strategic Priority Research Program (B) of the Chinese Academy of Sciences (Grant No. XDB04040300), the National Natural Science Foundation of China (Grant No. 11227902 and 11404359), and Shanghai Yang-Fan Program (Grant No. 14YF1407100). JZ was supported by the U.S. Department of Energy under Award DEFG02-08ER46544, the National Science Foundation under Grant No. ECCS-1408168, and the Theoretical Interdisciplinary Physics and Astrophysics Center.

* Electronic address: jiadongzang@gmail.com

- [1] U. K. Rößler, A. N. Bogdanov, and C. Pfleiderer, *Nature* **442**, 797 (2006).
- [2] S. Mühlbauer, B. Binz, F. Jonietz, C. Pfleiderer, A. Rosch, A. Neubauer, R. Georgii, and P. Böni, *Science* **323**, 915 (2009).
- [3] X. Z. Yu, Y. Onose, N. Kanazawa, J. H. Park, J. H. Han, Y. Matsui, N. Nagaosa, and Y. Tokura, *Nature* **465**, 901 (2010).
- [4] A. Fert, V. Cros, and J. Sampaio, *Nature Nanotechnology* **8**, 152 (2013).
- [5] X. Z. Yu, N. Kanazawa, Y. Onose, K. Kimoto, W. Z. Zhang, S. Ishiwata, Y. Matsui, and Y. Tokura, *Nature Materials* **10**, 106 (2011).
- [6] S. Seki, X. Z. Yu, S. Ishiwata, and Y. Tokura, *Science* **336**, 198 (2012).
- [7] I. Dzyaloshinskii, *Journal of Physics and Chemistry of Solids* **4**, 241 (1958).
- [8] T. Moriya, *Physical Review* **120**, 91 (1960).
- [9] M. Uchida, Y. Onose, Y. Matsui, and Y. Tokura, *Science* **311**, 359 (2006).
- [10] R. R. W. Birss, E. P., *Symmetry and Magnetism, Volume III* (North-Holland Publishing Company, 1964).
- [11] G. Kresse and J. Furthmüller, *Physical Review B* **54**, 11169 (1996).
- [12] J. P. Perdew, K. Burke, and M. Ernzerhof, *Physical Review Letters* **77**, 3865 (1996).
- [13] T. J. Prior, P. D. Battle, *Journal of Solid State Chemistry* **172**, 138 (2003).
- [14] T. J. Prior, S. E. Oldham, V. J. Couper, and P. D. Battle, *Chem. Mater.* **17**, 1867 (2005).
- [15] P. D. Battle, F. Grandjean, G. J. Longc, and S. E. Oldham, *J. Mater. Chem.* **17**, 4785 (2007).
- [16] A. F. Wells, *Three-dimensional Nets and Polyhedra*, Wiley, New York, 1977.
- [17] D. J. Singh, *Phys. Rev. B* **78**, 094511 (2008).
- [18] W. Li, J.-X. Zhu, Y. Chen, and C. S. Ting, *Phys. Rev. B* **86**, 155119 (2012).
- [19] H. J. Xiang, E. J. Kan, S.-H. Wei, M.-H. Whangbo, and X. G. Gong, *Phys. Rev. B* **84**, 224429 (2011).